PCCP

Accepted Manuscript

ROYAL SOCIETY OF CHEMISTRY

www.rsc.org/pccp

Journal Name

ARTICLE

Interaction of C_{60} fullerenes with asymmetric and curved lipid membranes: the molecular dynamics study

Received 00th January 20xx,
Accepted 00th January 20xx

DOI: 10.1039/x0xx00000x

www.rsc.org/

Yevhen K. Cherniavskyi [a], Christophe Ramseyer [b], Semen O. Yesylevskyy [a*]

Interaction of fullerenes with asymmetric and curved DOPC/DOPS bicelles is studied by means of coarse-grained molecular dynamics simulations. The effects caused by asymmetric lipid composition of the membrane leaflets and the curvature of the membrane are analyzed. It is shown that the aggregates of fullerenes prefer to penetrate into the membrane in the regions of moderately positive mean curvature. Upon penetration into the hydrophobic core of the membrane the fullerenes avoid the regions of extreme positive or negative curvature. The fullerenes increase the ordering of lipid tails, which are in direct contact with them, but do not influence other lipids significantly. Our data suggest that the effects of membrane curvature should be taken into account in the studies concerning permeability of the membranes to fullerenes and fullerene-based drug delivery systems.

Introduction

Discovery of the fullerenes in 1985 manifested the beginning of the carbon nanomaterials era which revolutionized the areas of material science and biomedical researches. Although other forms of carbon, such as nanotubes and graphene, are argued to be more promising for practical applications nowadays, the C_{60} fullerenes remain the most extensively studied carbon nanoparticles. Their nanometer size and unusual physical and chemical properties [1] make them suitable for numerous biomedical applications. The solubility and charge of the fullerenes can be routinely modified by chemical functionalization [2, 3]. Changes of the surface chemistry make them usable as anti-HIV, antitumor and antimicrobial agents as well as enzyme inhibitors [4-8], antibiotics [4, 6, 9, 10] and antioxidants [11]. The most promising application of the fullerenes is, however, their usage as drug delivery vectors [12]. The hydrophobic nature of the fullerenes and their very high affinity to the lipid membranes makes them promising drug carriers, which can transport polar or charged compounds into cells [13, 14]. Fullerenes are known to be toxic, which often limits their application in medicine. However, pure C_{60} molecules are more toxic than water-soluble functionalized forms [15].

The exact mechanisms of biological activity and toxicity of the C_{60} fullerenes are still subject to debate, which stimulated numerous computational studies of their interaction with biological membranes and macromolecules [16]. Early computational studies of the fullerenes were mainly focused on their aggregation in water [17] or behavior of individual fullerenes inside the lipid bilayer [18]. Recent studies of translocation of fullerenes through lipid membranes [19, 20] showed that pristine C_{60} fullerenes are trapped inside the hydrophobic core of the membrane which may cause toxicity by means of the membrane disruption [21].

Despite an obvious practical interest, no dedicated studied focused on the interaction of fullerenes with realistic models of eukaryotic cell membranes were performed to date. To our knowledge all computational studies done so far on the fullerenes in lipid membranes deal with planar symmetric lipid bilayers (add references here). Such simulation setup ignore two major properties of real cell membranes – their asymmetry and curvature [22, 23]. Living cells exhibit indeed various membrane shapes ranging from random undulations to highly curved protrusions and invaginations [24]. There are well-known experimental and theoretical studies of the membrane curvature [25-27] and bending elasticity [28], however only few dedicated simulations of the curved membranes are avilable. Most of them are related to membrane fusion [29-31] and the functioning of mechanosensitive ion channels [32] thus the curvature itself and its influence of the properties of bilayer are usually not analyzed in details.

The lipid composition of the membrane leaflets also differs dramatically. It is well known that phosphatidylcholine and sphyngomielin are located mostly in the outer leaflet of the plasma membranes, while phosphatidylethanolamine, phophatidylserine and phosphoinositides are abundant in the inner leaflet [33, 34]. The distribution of sterols, which are the most abundant molecules in eukaryotic membranes after the lipids, is also remarkably uneven [35-37]. Many important cellular phenomena such as formation of synaptic vesicles [27] and apoptotic bodies [38, 39], membrane fusion [40, 41], budding of

[a] Department of Physics of Biological Systems, Institute of Physics of the National Academy of Sciences of Ukraine, Prospect Nauky 46, Kiev-28, 03680, Ukraine.
[b] Laboratoire Chrono Environnement UMR CNRS 6249, Université de Bourgogne Franche-Comté, 16 route de Gray, 25030-Besançon, Cedex, France.
* Corresponding author: yesint4@gmail.com, Tel: +38 044 525 79 91.

enveloped viruses from the plasma membrane [42, 43], formation of blebs during apoptosis [38, 39], blood cell maturing [44] and mitosis [45] are known to be influenced by the lipid asymmetry and membrane curvature [46]. Thus, it is expected that interaction of the fullerenes with membranes is also dependent on the membrane curvature and asymmetry of their lipid composition.

In the present study we focus on the interaction of C_{60} fullerenes with curved and asymmetric DOPC/DOPS membranes. We constructed asymmetric bicelles with the leaflets containing DOPC and DOPS lipids, respectively. The middle of such bicelle possesses moderate spontaneous curvature caused by the lipid asymmetry, while the caps show extreme positive curvature. This allows to sample regions with very different curvature and lipid packing in only one simulation. Pure DOPC bicelles without spontaneous curvature were used as a reference in order to distinguish curvature and lipid composition effects. We used coarse-grained molecular dynamics simulations to simulate spontaneous penetration of the fullerenes from water phase to the bicelle and their distribution inside the hydrophobic core of the membrane at the time scale of tens of microseconds. To our knowledge, this work is the first systematic study of the interaction of fullerenes with asymmetric non-planar membranes.

Methods

Coarse-grained MARTINI force field version 2.1 [47] was used for all computations. C_{60} fullerene molecules were modeled according to the previous work of Monticelli et al. [48]. GROMACS software package versions 4.6.5 and 5.0.4 [49-51] was used. All simulations were performed at the temperature of 320 K with recommended simulation parameters for MARTINI force field [47]. Berendsen barostat with the relaxation constant of 5 ps was used for semi-isotropic pressure coupling. Pressure of 1 atm was maintained in Z direction while the size of the box in XY plane was fixed to prevent uncontrollable deformation of the simulation box.

An asymmetric bicelle consisted of neutral DOPC (dioleoylphosphatidylcholine), charged DOPS (dioleoylphosphatidylserine) lipids and cholesterol was constructed. Each monolayer of the bicelle was built from either DOPC or DOPS lipids (Figure 1). The bicelle is periodic in Z direction and has semi-cylindrical caps in XY plane. It is important to mention that the distribution of cholesterol molecules between the lipid monolayers can be significantly affected by initial setup, due to very large flip-flop transition time (up to few hundreds of ns) between the two leaflets in comparison with the total simulation time [22] (micro second time scale). Unbiased distribution of cholesterol molecules between the monolayers was obtained by following the e same method already used in our previous work [23]. C_{60} were initially placed between the membrane leaflets and were allowed to freely diffuse into the monolayers during the simulation.

The tails of DOPC and DOPS lipids are identical which leads to their spontaneous mixing both in experiments and in simulations with MARTINI force field. In our setup such mixing, which may occur by lateral diffusion through the caps of the bicelle, should be prevented in order to maintain the asymmetry between the monolayers. This is accomplished by introducing artificial repulsive potential between the coarse-grained phosphate groups of DOPC and DOPS lipids. This repulsive potential was implemented in the form of Lennard-Jones interactions with the interaction constants C_6=0, C_{12}=2.581 (GROMACS force field units). These parameters were already tested in our previous works [22]. They ensure that individual lipids almost never cross the boundary between the DOPC and DOPS domains. Small compact clusters of lipids of one type could sometimes diffuse into the domain of other lipid type (several such clusters are visible in Figure 1) but their number remains small at the time scale of tens of microseconds and they never distort the overall shape of the curved bicelle. Such clusters were excluded from analysis by considering only the lipids, which are surrounded by the nearest neighbors of the same type.

The bicelle was equilibrated for 10 μs. During equilibration, it developed significant curvature in XY plain due to different intrinsic curvatures of DOPC and DOPS lipids.

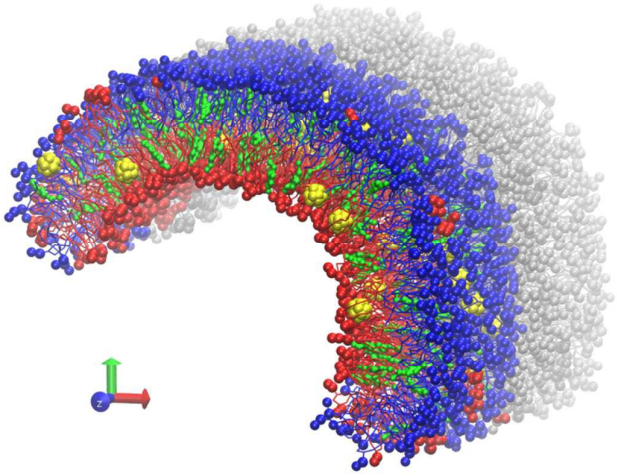

Figure 1. Equilibrated asymmetric DOPC/DOPS bicelle. DOPC lipids are blue, DOPS lipids are red, cholesterol molecules are green, individual fullerenes are yellow. Water is not shown for clarity. One of the periodic images of the system in Z dimension is shown in grey to emphasize that the bicelle is infinite in this direction.

After initial equilibration, 32 C_{60} fullerene molecules were randomly distributed in the water phase around the bicelle. The final system was composed of 504 DOPC lipids, 504 DOPS lipids, 196 cholesterol molecules, 32 C_{60} molecules , ~64000 coarse-grained water particles and 504 coarse-grained Na^+ ions to compensate the negative charges of DOPS lipid heads.

Five independent production simulations of the system with fullerenes were done. Each trajectory was 4 μs long (effective time). It is proved that effective time of simulations with coarse-grained MARTINI model is 4 times longer than real

simulation time [47]. In addition, the following reference trajectories were produced: 1) the 4 μs trajectory of DOPC/DOPS bicelle without fullerenes; 2) five independent trajectories of symmetric DOPC bicelle with fullerenes (1.5 μs each).

To compute local curvatures and instantaneous areas per lipid, the compiled C++ plug-in implemented in Pteros molecular modeling library [52] developed in our previous work [53] was used. The plug-in was modified in order to work with fullerene molecules. Its functionality was enhanced by adding ability to compute order parameter of the lipids tails taking into account local normal of the membrane.

The distributions of means and Gaussian curvatures shown in Figures 3-5 are computed by weighting local curvature at the position of particular lipid by the instantaneous areas occupied by this lipid at given simulation frame (see [53] for details).

Aggregation of the fullerenes was monitored by performing simple agglomerative clustering. The fullerene is considered to belong to a given cluster if the distance between its center of masses and the center of masses of any fullerene in the cluster is less than $2R+d$, where R=0.6 nm is the fullerene effective radius, d=0.01 nm. The mean cluster size was computed by averaging the size of all distinct clusters formed for each particular simulation frame.

To estimate influence of the fullerenes on the packing of lipids in asymmetric bicelle, order parameter for the lipid tails with respect to local normal of the bicelle was computed as :

$$S_z = \frac{3}{2}\langle cos^2\theta_z \rangle - \frac{1}{2}$$

where brackets denote time averaging over the trajectory; θ_z is the angle between the local membrane normal and the vector between two consecutive carbons in the tail. Order parameter can vary from 1 (full ordering along the interface normal) to -1/2 (full ordering in the tangent plane). Zero value corresponds to the case of isotropic orientation.

Results

Fig. 2 shows the evolution of the average size of the fullerene clusters in the course of simulations. The size of the clusters is one in the starting configuration because all fullerenes are added as single molecules. During the first ~50 ns, the average size of clusters increases rapidly due to very fast aggregation of fullerenes in the water phase. After this initial period, the clusters start penetrating into the bicelle. Then the clusters dissociate upon penetration which is clearly visible by the rapid decrease of their mean size. After the first ~700-1000 ns (depending on the trajectory), all fullerene clusters are absorbed by the bicelle and after ~1400 ns all clusters fall apart into individual molecules.

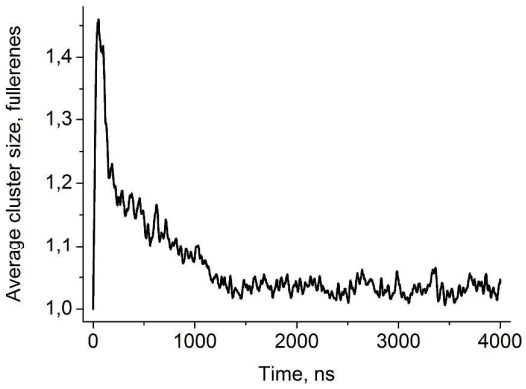

Figure 2. Average size of the fullerene clusters as a function of time. Presented curve is an average over five independent trajectories with different starting velocities. The curve is smoothed by moving window average (window size 50 ns) for clarity.

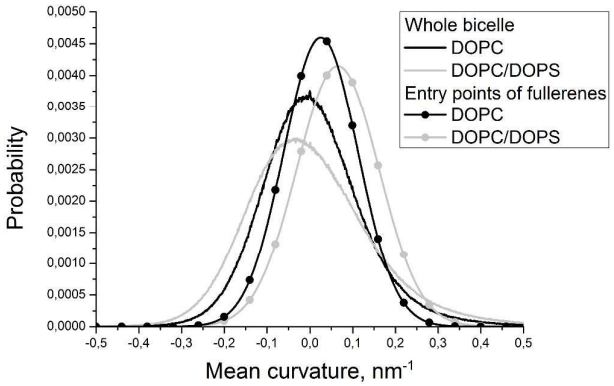

Figure 3. Distributions of the mean curvature for individual DOPC and DOPS monolayers and for the points of the first entry of fullerenes into these monolayers.

Figure 3 shows distributions of the mean curvature for four different cases: 1) for the points of the first entry of fullerenes into the asymmetric DOPC/DOPS bicelle; 2) for the whole DOPC/DOPS bicelle; 3) for the points of the first entry into the symmetric DOPC bicelle and 4) for the whole symmetric DOPC bicelle. The number of distinct first entry events is only 160 (32 fullerenes in 5 independent trajectories) for each system thus we computed first and second statistical moments of the distribution (mean value and dispersion) and plotted corresponding approximated Gaussian distribution in Fig. 3.

The maximum of distribution for symmetric DOPC bicelle is centered at zero, while the distribution for DOPC/DOPS is shifted slightly to positive curvatures. This is explained by the larger surface area of the convex DOPC monolayer and the presence of the caps with positive mean curvature (the curvatures are weighted by the instantaneous area per lipid as explained in the Methods section). The distributions in the points of the first entry are shifted substantially to positive curvatures in comparison with the corresponding distributions for the whole bicelles in both systems. The magnitude of this shift is very similar in asymmetric and symmetric bicelles which

means that this effect is systematic and not caused by the presence of artificial repulsive potential in the asymmetric bicelle.

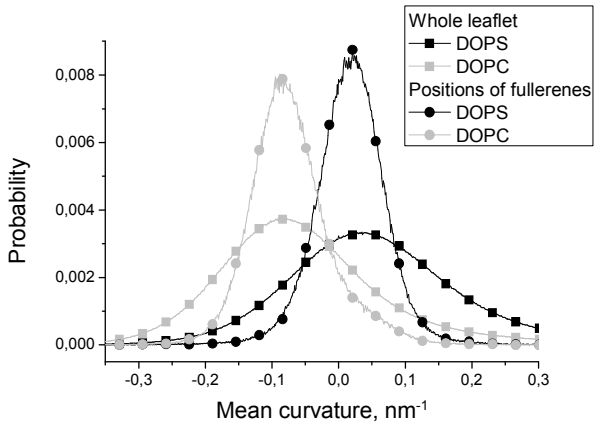

Figure 4. Distributions of the local mean curvature in the whole DOPC and DOPS leaflets and in the positions of the fullerenes in these leaflets.

Figure 4 compares distributions of mean curvature in the points where fullerenes are located in equilibrium with the distributions for the whole DOPC and DOPS monolayers. The maxima of the distributions for the fullerenes and for the whole monolayers almost coincide for both DOPC and DOPS lipids. However, the half-widths of the distributions for fullerenes are much smaller in comparison with the distributions for corresponding monolayers. This clearly shows that the fullerenes concentrate in the regions which have the curvature close to average curvature for particular monolayer and avoid the regions with unusually large or unusually small curvature.

The fullerenes are distributed almost uniformly between different monolayers in equilibrium (51% in DOPC monolayer and 49% in DOPS monolayer) despite the fact that convex DOPC monolayer has large surface area.

Figure 5 shows distribution of the Gaussian curvature in the equilibrium positions of fullerenes and for the whole bicelle. The distributions are not subdivided into DOPC and DOPS monolayers because they are essentially identical for both of them (data not shown). The maxima of both distributions coincide and equal to zero while their widths show the same behavior as the distributions of mean curvature in Fig. 4. The distribution for the fullerenes is significantly narrower which means that the fullerenes avoid the regions of very large or very small Gaussian curvature in the same way as they do this in the case of mean curvature.

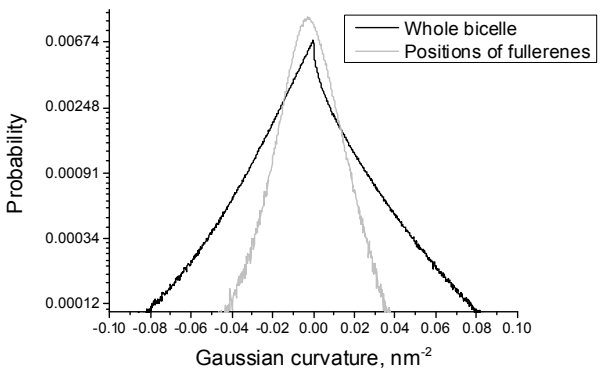

Figure 5. Distributions of the local Gaussian curvature in the whole bicelle and in the positions of fullerenes for asymmetric DOPC/DOPS bicelle.

Figure 6 shows distribution of the distance from the bicelle's surface to the fullerene molecules. There are two peaks on this distribution but only one of them (the one close to the surface of the membrane) is significant while the other one is an artifact caused by the coarse-grained force field (see Discussion for details). This distribution is essentially the same for DOPC and DOPS monolayers of the asymmetric bicelle and for symmetric DOPC bicelle (data not shown).

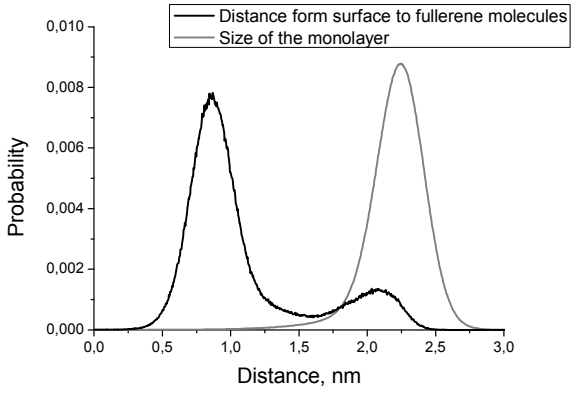

Figure 6. Distributions of the distance from membrane's surface to the fullerene molecules (black line) and monolayer size (gray line).

In order to estimate the influence of fullerences on the shape of asymmetric DOPC/DOPS bicelle, we compared the distributions of mean and Gaussian curvatures for the systems with and without fullerenes (figures 7 and 8). It is clearly seen that addition of the fullerenes does not lead to any significant change of these distributions which means that the fullerenes do not change the overall shape and curvature of the bicelle.

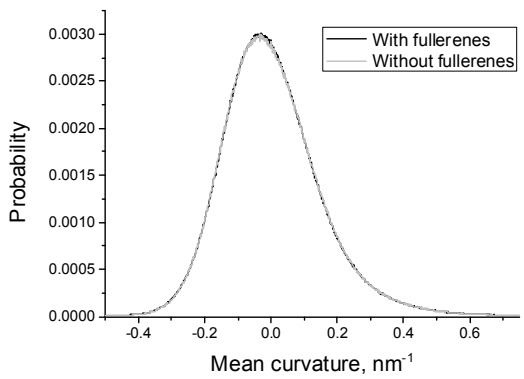

Figure 7. Distributions of the mean curvature of the DOPC/DOPS bicelle with and without fullerenes.

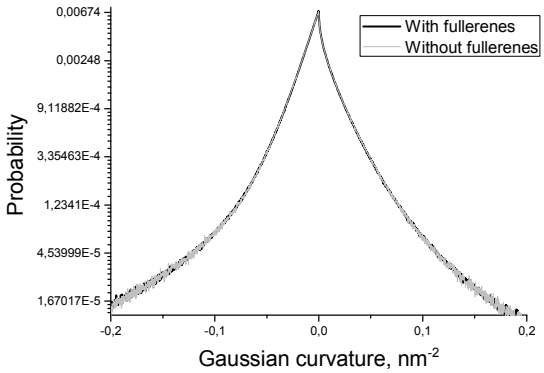

Figure 8. Distributions of the Gaussian curvature of the DOPC/DOPS bicelle with and without fullerenes.

Despite the fact that the fullerenes do not change the curvature of the bicelle, they influence the packing of individual lipid chains. Figure 9 shows the orientaional order parameter for the lipid tails which are in direct contact (within 0.6 nm) with the fullerenes and those which are far from them. Tails of the DOPC and DOPS lipids are represented by six coarse-grained beads in MARTINI force field. Every point on the plot represents an order parameter of the vector, which connects two neighboring coarse-grained particles counting from the lipid head. It is clearly seen from Figure 9 that ordering of the first particles of the lipid tails increases for the lipids, which are in contact with the fullerenes.

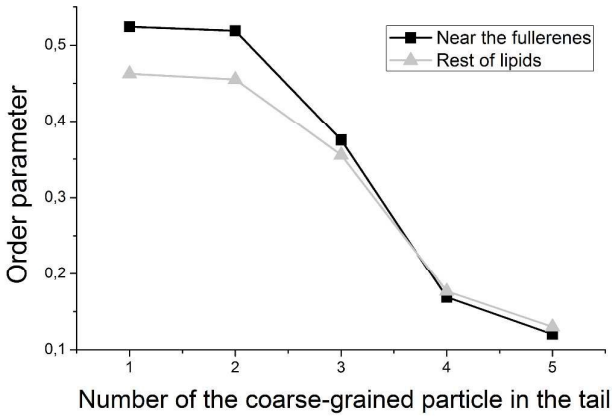

Figure 9. Order parameter of the lipid tails, computed for the lipids near (black line) and far (gray line) from the fullerenes inside of the bicelle.

Discussion

Aggregation of the fullerenes

Fullerene molecules are hydrophobic by nature and tend to aggregate in aqueous solution. In our simulations, 32 individual fullerene molecules were initially placed at random positisions in water phase. In the course of simulation, there is a competition between aggregation of fullerenes in water and their incorporation into the bicelle. Aggregation dominates in the first ~50 ns of simulations when the average size of clusters increases rapidly. After this initial period, the clusters start colliding with the bicelle and penetrating into its hydrophobic core. Visual inspection shows that the clusters of fullerenes penetrate into the bicelle without dissociation. Rather big clusters of up to 5-7 fullerenes can enter the bicelle. Upon penetration to the lipid bilayer, the clusters start dissociating into individual molecules. This process finishes completely after ~1400 ns. Equilibrium size of the clusters is slightly larger than one due to random collisions of the fullerenes inside the hydrophobic core of the bicelle. Such collisions are transient and do not lead to aggregation.

Curvature-dependent penetration of the fullerenes

In order to study the role of mean curvature in the process of penetration of the fullerenes into the lipid bilayer, we analyzed the points of their first entry into the bicelle. The data obtained from five independent simulations of asymmetric DOPC/DOPS and symmetric DOPC bicelles were collected to account for the role of asymmetric lipid distribution.

The fact that distribution of the mean curvature of pure DOPC bicelle is centered at zero (Fig. 3) is expected since symmetric bicelle does not develop any significant curvature except of random undulations. The only regions of large positive mean curvature are cylindrical caps of the bicelle. In the case of asymmetric DOPC/DOPS bicelles the peak of the mean curvature distribution is shifted towards positive curvatures due to the fact that the asymmetric bicelle is significantly curved as a whole and the convex DOPC monolayer has larger surface area.

The distributions of the mean curvature in the points of the first entry of fullerenes are shifted significantly to more positive values for both symmetric and asymmetric bicelles (Fig. 3). This clearly indicates that the fullerenes prefer to penetrate through the convex membrane surface with positive mean curvature where the distances between the lipid head groups are larger than in the concave surface with negative mean curvature.

Visual inspection of trajectories shows that the majority of entry events occur far from the bicelle caps in the regions of moderately positive mean curvature. In the case of asymmetric bicelle the number of entries through the caps is significantly higher. This could be attributed to the repulsion between DOPC and DOPS lipids which prevents their spontaneous mixing in the caps of the bicelle but increases the distance between their head groups. If one excludes extra penetration events through the bicelle caps caused by this artifact then both symmetric and asymmetric bicelles show very similar behavior.

It is possible to conclude that the fullerenes prefer to penetrate into the membrane displaying regions with positive local mean curvature. In contrast, preferred positions of penetration into the bicelle are not sensitive to local Gaussian curvature (data not shown).

Equilibrium distribution of the fullerenes inside the bicelle

According to Fig. 4, equilibrium distribution of the fullerenes inside the bicelle is not significantly influenced by the mean curvature except the slight preference for negative mean curvatures (concave surfaces) in DOPS monolayer. However, it is clearly seen that only negligible amount of fullerenes is located in the regions with extreme values (either positive or negative) of mean curvature. Thus, we can conclude that the fullerenes are distributed almost evenly in the regions with moderate curvature and avoid the regions with extreme curvature (including the bicelle caps).

Fig. 5 shows that the equilibrium distribution of fullerenes is independent of the local Gaussian curvature. The sharp peak obtained in the distribution of the Gaussian curvature near zero confirms that most of the membrane has cylinder-like topology imposed by the system setup (the membrane is infinite in Z dimension).

Another important characteristic of equilibrium fullerene distribution inside the bicelle is their distance from the membrane surface (Figure 6). Two distinct populations of the fullerenes exist: the major one at ~0.9 nm from the surface, and the minor one at approximately 2.1 nm. The major population is located at the the beginning of the lipid tails just underneath the head groups. The minor population is located at the center of the bilayer but it is proved to be an artifact of the coarse-grained MARTINI force field for the fullerenes [48]. Indeed, the potentials of mean force (PMF) for transferring fullerenes across the membrane in all-atom simulations show a single energy well, which coincides with our major population [48]. However, coarse-grained PMF with MARTINI force field shows very small additional energy well in the center of bilayer which leads to the appearance of minor population [48]. The minor population in the center of bilayer is ignored in our analysis. Appearance of such small artifacts in energy profiles is a usual trade-off of the coarse grained force fields which is almost impossible to avoid during parameterization. In the case of our system small additional population of the fullerenes in the center of bilayer is harmless since the fullerenes in general do not influence overall shape and curvature of the bicelle, which is apparent from the Figures 7 and 8.

Ordering of the lipid tails

It is expected that the presence of large fullerene molecules in the membrane should affect the ordering of the lipid tails significantly. However, in the previous works which utilized MARTINI force field [19], the authors did not observe any significant changes in the average order parameter of the lipid tails in the presence of fullerenes. Detectable changes in the order parameter were only observed for very high concentrations of the fullerene molecules (~11% molar concentration). In this work, we studied ordering of the lipid tails in more details by computing an order parameter for the lipid tails, which are in direct contact with the fullerenes and for the rest of the lipid tails separately. Figure 9 shows that the tails of the lipids, which are in direct contact with the fullerenes, are significantly more ordered in the region close to the head groups. This is in perfect agreement with the average location of the fullerenes in the bilayer in this region (Fig. 6) and suggests that the fullerenes induce additional ordering of the lipid tails in their local vicinity but do not influence remote lipids significantly.

Conclusions

In this work, we studied interaction of asymmetric DOPC/DOPS bicelles with C_{60} fullerenes using coarse-grained molecular dynamics simulations. We performed a series of simulations of DOPC/DOPS bicelles with fullerenes in water and compared the results with the simulation of symmetric DOPC bicelles in order to distinguish the effects of the membrane asymmetry and curvature.

It is shown that the fullerenes form stable aggregates in water which penetrate into the membrane as a whole. However, such clusters dissociate quickly into separate molecules inside the membrane.

Our data show that the fullerenes prefer to penetrate into the membrane in the regions with positive mean curvature. This preference is observed in symmetric and asymmetric bicelles alike.

The fullerenes are distributed almost equally in the regions with moderate curvature inside the membrane. However, they strongly avoid the regions with extreme positive or negative curvatures. Also neither mean nor Gaussian curvature of the bicelle itself is changed significantly in the presence of fullerenes at ~3.2% molar concentration.

The fullerene molecules significantly increase the order parameter of the lipid tails which are in direct contact with

them. At the same time, the ordering of the lipids which are not in contact with the fullerenes is not affected.

Our data clearly shows that behavior of the fullerenes in asymmetric and curved membranes is non-trivial. The effects of the curvature are more pronounced in comparison with the effects of lipid composition of the membrane leaflets. Penetration of the fullerenes into the membranes and their distribution in the hydrophobic part of the bilayer are curvature-dependent and should be taken into account in the studies concerning permeability of the membranes to fullerene-based drug delivery systems.

Acknowledgements

S.Y. and Y.C. thank the Université de Bourgogne Franche-Comté for financial support. The authors thank the Mésocentre de calcul de Franche-Comté for providing computational resources for this work.

Notes and references

1. T. Da Ros and M. Prato, *Chem. Commun.*, 1999, 8, 663-669.
2. M. Brettreich and A. Hirsch, *Tetrahedron Lett.*, 1998, 39, 2731-2734.
3. A. Hirsch, *Nature Mat*, 2010, 9, 868–871.
4. S. Bosi, T. Da Ros, G. Spalluto and M. Prato, *Eur J Med Chem*, 2003, 38, 913–923
5. R. Bakry, R. M. Vallant, M. Najam-ul-Haq, M. Rainer, Z. Szabo, C. W. Huck and G. K. Bonn, *Int J Nanomed*, 2007, 2, 639–649.
6. S. Nakamura and T. Mashino, *J Phys: Conf Ser*, 2009, 159, 012003.
7. G. D. Nielsen, M. Roursgaard, K. A. Jensen, S. S. Poulsen and S. T. Larsen, *Basic Clin Pharmacol Toxicol*, 2008, 103, 197–208.
8. R. Partha and J. L. Conyers, *Int J Nanomed*, 2009, 4, 261–275.
9. T. Mashino, K. Okuda, T. Hirota and M. Hirobe, *Bioorg Med Chem Lett*, 1991, 9, 2959–2962.
10. H. Aoshima, K. Kokubo, S. Shirakawa, M. Ito, S. Yamana and T. Oshima, *Biocontrol Sci*, 2009, 14, 69–72.
11. I. C. Wang, L. A. Tai, D. D. Lee, P. P. Kanakamma, C. K. F. Shen, T.-Y. Luh, C. H. Cheng and K. C. Hwang, *Journal of medicinal chemistry*, 1999, 42, 4614-4620.
12. R. Partha and J. L. Conyers, *Int. J. Nanomed.*, 2009, 4, 261-275.
13. R. Partha, L. R. Mitchell, J. L. Lyon, P. P. Joshi and J. L. Conyers, *ACS Nano*, 2008, 2, 1950-1958.
14. L. L. Dugan, D. M. Turetsky, C. Du, D. Lobner, M. Wheeler, C. R. Almli, C. K. F. Shen, T. Y. Luh, D. W. Choi and T. S. Lin, *Proc. Natl. Acad. Sci. U. S. A.*, 1997, 94, 9434-9439.
15. C. M. Sayes, J. D. Fortner, W. Guo, D. Lyon, A. M. Boyd, K. D. Ausman, Y. J. Tao, B. Sitharaman, L. J. Wilson, J. B. Hughes, J. L. West and V. L. Colvin, *Nano letters*, 2004, 4, 1881-1887.
16. D. Bedrov, G. D. Smith, H. Davande and L. Li, *J. Phys. Chem. B*, 2008, 112, 2078-2084.
17. N. Choudhury, *The Journal of chemical physics*, 2006, 125, 034502-034507.
18. L. Li, H. Davande, D. Bedrov and G. D. Smith, *The Journal of Physical Chemistry B*, 2007, 111, 4067-4072.
19. J. Wong-Ekkabut, S. Baoukina, W. Triampo, I. M. Tang, D. P. Tieleman and L. Monticelli, *Nat Nano*, 2008, 3, 363-368.
20. S. O. Yesylevskyy, S. Kraszewski, F. Picaud and C. Ramseyer, *Molecular Membrane Biology*, 2013, 30, 338-345.
21. C. Cusan, T. Da Ros, G. Spalluto, S. Foley, J. M. Janto, P. Seta, C. Larroque, M. C. Tomasini, T. Antonelli, L. Ferraro and M. Prato, *Eur. J. Org. Chem.*, 2002, 17, 2928-2934.
22. S. Yesylevskyy and A. Demchenko, *Eur Biophys J*, 2012, 41, 1043-1054.
23. S. O. Yesylevskyy, A. P. Demchenko, S. Kraszewski and C. Ramseyer, *The Scientific World Journal*, 2013, 2013, 10.
24. H. T. McMahon and J. L. Gallop, *Nature*, 2005, 438, 590-596.
25. D. Marsh, *Biophys. J*, 1996, 70, 2248-2255.
26. Y. Shibata, J. Hu, M. M. Kozlov and T. A. Rapoport, *Annual Review of Cell and Developmental Biology*, 2009, 25, 329-354.
27. H. T. McMahon, M. M. Kozlov and S. Martens, *Cell*, 2010, 140, 601-605.
28. D. Marsh, *Chem. Phys. Lipids*, 2006, 144, 146-159.
29. S. Martens and H. T. McMahon, *Nat Rev Mol Cell Biol*, 2008, 9, 543-556.
30. V. Knecht and S.-J. Marrink, *Biophys. J*, 2007, 92, 4254-4261.
31. S. Marrink and A. Mark, *Journal of the American Chemical Society*, 2003, 125, 11144-11145.
32. G. R. Meyer, J. Gullingsrud, K. Schulten and B. Martinac, *Biophys. J*, 2006, 91, 1630-1637.
33. V. Kiessling, C. Wan and L. K. Tamm, *Biochim Biophys Acta*, 2009, 1788, 64-71.
34. A. P. Demchenko and S. O. Yesylevskyy, *Chem Phys Lipids*, 2009, 160, 63-84.
35. M. R. Ali, K. H. Cheng and J. Huang, *Proc Natl Acad Sci U S A*, 2007, 104, 5372-5377.
36. A. Radhakrishnan and H. McConnell, *Proc Natl Acad Sci U S A*, 2005, 102, 12662-12666.
37. H. Ohvo-Rekila, B. Ramstedt, P. Leppimaki and J. P. Slotte, *Prog Lipid Res*, 2002, 41, 66-97.
38. G. J. Gores, B. Herman and J. J. Lemasters, *Hepatology*, 2005, 11, 690-698.
39. R. C. Taylor, S. P. Cullen and S. J. Martin, *Nature Reviews Molecular Cell Biology*, 2008, 9, 231-241.
40. R. Jahn, T. Lang and T. C. Südhof, *Cell*, 2003, 112, 519-533.
41. M. A. Churchward, T. Rogasevskaia, J. Höfgen, J. Bau and J. R. Coorssen, *Journal of cell science*, 2005, 118, 4833-4848.
42. T. L. Cadd, U. Skoging and P. Liljeström, *Bioessays*, 2005, 19, 993-1000.
43. M. Lorizate and H.-G. Kräusslich, *Cold Spring Harb Perspect Biol* 2011, 3, a004820.
44. R. E. Griffiths, S. Kupzig, N. Cogan, T. J. Mankelow, V. M. S. Betin, K. Trakarnsanga, E. J. Massey, J. D. Lane, S. F. Parsons and D. J. Anstee, *Blood*, 2012, 119, 6296-6306.
45. C. Roubinet, B. Decelle, G. Chicanne, J. F. Dorn, B. Payrastre, F. Payre and S. Carreno, *JCB*, 2011, 195, 99-112.
46. W. B. Huttner and J. Zimmerberg, *Current opinion in cell biology*, 2001, 13, 478-484.
47. S. J. Marrink, H. J. Risselada, S. Yefimov, D. P. Tieleman and A. H. de Vries, *The Journal of Physical Chemistry B*, 2007, 111, 7812-7824.
48. L. Monticelli, *Journal of chemical theory and computation*, 2012, 8, 1370-1378.
49. B. Hess, C. Kutzner, D. van der Spoel and E. Lindahl, *Journal of chemical theory and computation*, 2008, 4, 435-447.
50. S. Páll, M. Abraham, C. Kutzner, B. Hess and E. Lindahl, in *Solving Software Challenges for Exascale*, eds. S. Markidis and E. Laure, Springer International Publishing, 2015, vol. 8759, ch. 1, pp. 3-27.
51. S. Pronk, S. Páll, R. Schulz, P. Larsson, P. Bjelkmar, R. Apostolov, M. R. Shirts, J. C. Smith, P. M. Kasson, D. van der Spoel, B. Hess and E. Lindahl, *Bioinformatics*, 2013, 29, 845-854.
52. S. O. Yesylevskyy, *Journal of computational chemistry*, 2015, 36, 1480-1488.
53. S. O. Yesylevskyy and C. Ramseyer, *Physical Chemistry Chemical Physics*, 2014, 16, 17052-17061.